Half the world's population already experiences years 1.5°C warmer than preindustrial

Summary: We develop a gridded temperature exposure dataset that incorporates both the urban heat island effect and changes between the early industrial and preindustrial.

Chris Brierley[1*], Alexander Koch[1], Maryam Ilyas[2,3], Natalie Wennyk[1], and Jarmo Kikstra[1]

[1]Department of Geography, University College London, London, U.K.
[2]Department of Statistical Science, University College London, London, U.K.
[3]College of Statistical and Actuarial Sciences, University of the Punjab, Lahore, Pakistan

[*]To whom correspondence should be addressed; E-mail: c.brierley@ucl.ac.uk.

The Paris Agreement aims to limit the increase in global average temperature to 1.5 °C above preindustrial. A natural question for the public to ask is "But how much warmer than preindustrial is where I live?" We develop a pattern-scaling technique to present local annually-resolved, gridded temperature anomalies prior to the industrial burning of fossil fuels. On average the past 5 years, 2014-2018, was 1.13 °C above preindustrial (with a likely range of 1.00-1.26 °C). When accounting for the distribution of the human population and urban heat island effect, we find that people experienced an average warming of 1.61 °C (1.43-1.79 °C) over the same period. When the Paris Agreement was signed in 2015, the majority of the global population was ex-

posed to local, annual temperatures warmer than 1.5 °C above preindustrial.

The world has warmed appreciably over the past two centuries (Fig. 1a). The Paris Agreement commits the world to keeping global mean temperature 'well-below 2 °C' above preindustrial (*1*). This value is a global average and some regions will experience warming much greater than this, for example the Arctic (*2*). Such a regional pattern can make it hard for people to associate the global target with their local experiences (*3*). The long timescales of climate change provide a further challenge: not only does interannual variability obscure the multi-year average, but the preindustrial reference state was multiple generations ago (*4*).

Regional temperature changes are rarely presented with respect to the preindustrial. For example, they were never shown this way in the IPCC's 5th Assessment Report (*5*), upon which the Paris Agreement was grounded. The recent IPCC special report "Global Warming of 1.5 °C" was the first to show temperature plots with respect to a preindustrial baseline (*6*). Choosing not to present changes from preindustrial may be justified given the uncertainty in our knowledge of the preindustrial baseline (for example Fig. 1b implies less confidence in warming trend than Fig. 1a). However, it may mislead causal observers about the magnitude of warming that has occurred. Here we provide and display an ensemble of gridded temperature observations that shows the local warming since preindustrial and its uncertainty.

The sparse instrumental coverage prior to the 1950s means that even the state of the El Niño-Southern Oscillation may be ambiguous (*7*), despite being the dominant mode of climate variability (*8*). This means that when calculating regional temperature changes from any preindustrial baseline one must also formally quantify the uncertainties, especially those associated with the regions without instrumental coverage (*9*). Here we base our dataset on the HadCRUT4 compilation of station observations (*10*) combined with multi-resolution lattice kriging (*9*) to retain covariance relationships at global, synoptic and local scales. 10,000 equally-plausible ensemble members represent the observed temperature change, beginning in 1850 CE (*7*) (Methods).

The Paris Agreement does not provide a precise definition of when the preindustrial reference period occurred (*1*). For practical reasons, the early industrial (1850–1900 CE) is used as a fair approximation (*5, 6*), because this is earliest that we have sufficient global coverage of instrumental records. An earlier reference period would be desirable from a radiative forcing perspective (*11*), because humans had already noticeably altered the climate system by the early instrumental period (*12, 13*). An expert assessment states that the earlier reference period was cooler than the 1850–1900 CE instrumental period (*6, 11*), with a subsequent model-based quantification of 0.079 °C (likely range of -0.025 to 0.184 °C) cooler (*14*)(Methods). The uncertainty in the preindustrial baseline temperature even propagates into the estimate of well-observed years (*11*) (Fig. 1b). There is ongoing discussion about the most appropriate definition of the preindustrial baseline (*15,16*). Here we apply the stricter definition of a long-term average climate prior to industrialisation (*14*) (taken as 1400–1800 CE, Methods), rather than assume the early instrumental period (1850–1900 CE) represents "preindustrial" conditions (*5, 6*).

Reconstructing the spatial pattern of the warming prior to reliable instrumental coverage (pre-1850 CE) presents a different challenge. The forced component of global warming of the early instrumental period (1850–1900 CE) with respect to 1400–1800 CE has been estimated from a 26-member multi-model ensemble of climate simulations covering the past millennium (*14*). The global mean warming is often used as an index of climate change, because local temperature changes and some impacts scale approximately linearly with it (*17, 18*). Unfortunately conventional pattern-scaling tools are not appropriate to expand the global mean offsets spatially, because they either cannot represent cold states prior to the future projections (*18*) or do not allow realistic covariance sampling (*17*).

Here we adopt a novel pattern-scaling approach that not only reconstructs the mean pattern and local uncertainty, but critically also retains the spatial covariances between locations in its reconstructed patterns (Methods). In brief, an ensemble of scalable patterns were created from the regression slopes of the first 10 empirical orthogonal functions of the merged surface temperatures changes seen in CMIP5 under the RCP2.6 scenario (Fig. S1, combined with a residual term. We multiply these scalable patterns by the global mean warming from the preindustrial to the early instrumental (*14*) to estimate the temperature offset between these two periods (Fig. 2A). The uncertainty in the preindustrial offset (Fig. 2B) is substantially less than the uncertainty in the early industrial observations (predominantly arising from incomplete global coverage), which itself is of a similar magnitude to interannual variability (Methods). Combining the offset estimates with the spatially-complete temperature observations (*7*), we create an annual-resolution dataset of local temperature anomalies from the preindustrial along with quantified uncertainties (Methods).

On average, the past five years (2014-2018) was significantly warmer than preindustrial across the majority of the globe (Fig. 2F). The proportion of the globe with temperature anomalies greater than 1.5 °C was 27.3% (likely range 22.5–32.4%); and 14.1% (10.9–17.4%) saw temperatures over 2 °C (Fig. 3A, Tab. S2).

As well as temperatures rising since the preindustrial, the global population has increased dramatically (*19*) (Fig. 3b). People are not evenly spread across the globe (Fig. S2): the vast majority live on the land, which warms faster the ocean (*20*). Assessing the direct health impacts of the warming requires consideration of only the temperatures to which people are exposed - rather than the global average (*21*). The majority of the world's population lives in Asia (*19*), yet very few live in the portion of Asia with the warmest temperature anomalies (Siberia was more than 2.5 °C above preindustrial; Fig. 2F).

A further major demographic trend over the past two centuries has been the shift to living in towns and cities instead of the countryside (*19*). Due to the urban heat island effect (*22*), this shift itself will lead to people on average being exposed to higher temperatures (Fig. S2. Whilst estimates of the urban heat island effect exist with global coverage (*23*), information about of their evolution since 1850 CE does not. We therefore incorporate the impact of urbanisation as a time invariant adjustment felt by an increasing proportion of the population (Methods).

Combining the temperature dataset with both population information and the urbanisation adjustments allows the number of people living at various warming levels to be determined each year (Fig. 3a). The total number of people that experience an annual mean temperature at, or below, the preindustrial level in each year has not increased, despite the substantial population growth (Fig. 3a). As a percentage however, it has dropped throughout the industrial era and is effectively negligible now (Fig. 4). It is as if all the population growth since industrialisation has occurred at elevated temperatures. Resilience to climate change may be better measured with respect to interannual variability (*24*), with a shift of more than two standard deviations (Fig. 2) termed an unfamiliar climate (*25*). Few people now live at temperatures 'familiar' to the preindustrial (Fig. S4).

The Lancet Countdown (*21*) defines one indicator for the health effects of temperature change as the 'exposure-weighted' average temperature (i.e. the temperature change experienced by a person on average). The report stressed that this indicator increased at double the rate of global (area-weighted) temperature since 2000 CE (*21*). The temperature anomaly dataset and urban heat island methodology developed here means it is possible to 'exposure-weight' the warming since the preindustrial for the first time. This indicator consistently shows larger changes with respect to the preindustrial (Fig. 1c) than the global mean temperature since 1850 CE (Fig. 1b). This occurs as the human population is not distributed evenly over the globe (*19*) and urbanisation exposes people to warmer temperatures (*22*) (Fig. S2).

The impact of considering the relative population sizes when thinking about observed temperature changes across the globe are best illustrated through the use of cartograms (*25, 26*). Fig. 4 presents the national average warming since the preindustrial for 2014–2018: using

(A) area weighting and (B) both exposure-weighting and scaling each country's size relative to its national population. The differing impacts of considering the exposure-weighted and area-weighted averages is most noticeable in North America.

Natural year-to-year variations can mean there are always regions of the globe that experience temperature at or below the preindustrial, as well as substantially warmer than that (Fig. 2) Nonetheless as the global population crossed 2 billions in the 1930s, it also crossed into a world where, for the first time, less people were exposed to a preindustrial climate than a world with warming of 1 °C or higher (Fig. 4). Our analysis shows that 1990 CE was the first year that 50% of the world's population was exposed to 1 °C above preindustrial, albeit temporarily. Since the Kyoto Protocol was signed in 1997 CE, a majority of the world's population has lived with annual temperatures 1 °C or more above preindustrial (Fig. 4). We find that in 2015 CE over half of the global population was exposed to temperatures greater than 1.5 °C above preindustrial (55%, Tab. S2).

The Paris Agreement (*1*) commits us to "pursuing efforts to limit [global average] temperature increase to 1.5 °C". The Paris target should be interpreted as excluding natural variations (*27*). The ensemble of patterns used to create the preindustrial baseline can also be scaled to represent the regional temperatures associated with various global mean temperatures. This allows estimation of the amount of people that experienced local temperatures equivalent to a global mean temperature rise of 1.5 °C (Fig. S4). Our median estimate for 2015 is that half of world's population experienced annual mean temperatures equivalent to a global warming of 1.5 °C above preindustrial - a third of whom only did so because of urban heat island effects (Tab. S2).

The Paris Agreement is highly, yet necessarily, ambitious in its desire to limit temperature to 1.5 °C above preindustrial (*1*). While the reference to a preindustrial baseline is justifiable, it introduces additional uncertainty into the observed temperature increases (*11, 15, 16*). Having devised a methodology to account for the local expression of this uncertainty, we explore the spatial pattern of temperature changes from both geographic and demographic perspectives. Most people alive today are unlikely to have ever experienced preindustrial temperatures, especially given an increasing urban population exposed to urban heat island effects. Indeed the majority of the world's population has already experienced annual temperatures above 1.5 °C, and the remainder is likely to experience temperatures equivalent to a 1.5 °C world much earlier than the planet itself (*25*). Given the global population's current exposure to warmer temperatures, and the fact that health impacts are often related to that exposure (*21*), it is clear that we should stop thinking of climate change primarily in the future tense.

References

1. United Nations Framework Convention on Climate Change, *Adoption of the Paris Agreement FCCC/CP/2015/10/Add.1* (2015).

2. M. C. Serreze, R. G. Barry, *Global and planetary change* **77**, 85 (2011).

3. P. D. Howe, E. M. Markowitz, T. M. Lee, C.-Y. Ko, A. Leiserowitz, *Nature Climate Change* **3**, 352 (2013).

4. M. Hulme, S. Dessai, I. Lorenzoni, D. R. Nelson, *Geoforum* **40**, 197 (2009).

5. D. L. Hartmann, *et al.*, *Climate Change 2013 the Physical Science Basis: Working Group I Contribution to the Fifth Assessment Report of the Intergovernmental Panel on Climate Change* (Cambridge University Press, 2013).

6. M. Allen, *et al.*, *Global Warming of 1.5°C: an IPCC special report* (Cambridge University Press, 2018).

7. M. Ilyas, C. M. Brierley, S. Guillas, *Geophysical Research Letters* **44**, 9068 (2017). 2017GL074596.

8. B. Huang, M. L'Heureux, Z.-Z. Hu, H.-M. Zhang, *Geophysical Research Letters* **43**, 9165 (2016).

9. D. Nychka, S. Bandyopadhyay, D. Hammerling, F. Lindgren, S. Sain, *Journal of Computational and Graphical Statistics* **24**, 579 (2015).

10. C. P. Morice, J. J. Kennedy, N. A. Rayner, P. D. Jones, *Journal of Geophysical Research: Atmospheres* **117**, n/a (2012). D08101.

11. E. Hawkins, *et al.*, *Bulletin of the American Meteorological Society* (2017).

12. A. P. Schurer, G. C. Hegerl, M. E. Mann, S. F. Tett, S. J. Phipps, *Journal of Climate* **26**, 6954 (2013).

13. A. Koch, C. Brierley, M. M. Maslin, S. L. Lewis, *Quaternary Science Reviews* **207**, 13 (2019).

14. A. P. Schurer, M. E. Mann, E. Hawkins, S. F. Tett, G. C. Hegerl, *Nature Climate Change* **7**, 563 (2017).

15. A. Schurer, *et al.*, *Nature Geoscience* **11**, 220 (2018).

16. R. J. Millar, *et al.*, *Nature Geoscience* **11**, 222 (2018).

17. T. J. Osborn, C. J. Wallace, I. C. Harris, T. M. Melvin, *Climatic Change* **134**, 353 (2016).

18. C. Tebaldi, J. M. Arblaster, *Climatic Change* **122**, 459 (2014).

19. K. K. Goldewijk, A. Beusen, J. Doelman, E. Stehfest, *Earth System Science Data* **9**, 927 (2017).

20. M. M. Joshi, J. M. Gregory, M. J. Webb, D. M. Sexton, T. C. Johns, *Climate Dynamics* **30**, 455 (2008).

21. N. Watts, *et al.*, *The Lancet* **391**, 581 (2018).

22. T. R. Oke, *Quarterly Journal of the Royal Meteorological Society* **108**, 1 (1982).

23. Center for International Earth Science Information Network, Columbia University, Global urban heat island (UHI) data set, 2013 (2016).

24. F. Lehner, T. F. Stocker, *Nature Climate Change* **5**, 731 (2015).

25. D. Frame, M. Joshi, E. Hawkins, L. J. Harrington, M. de Roiste, *Nature Climate Change* **7**, 407 (2017).

26. D. Dorling, A. Barford, M. Newman, *IEEE Trans. Vis. Comput. Graph.* **12**, 757 (2006).

27. J. Rogelj, C.-F. Schleussner, W. Hare, *Geophysical Research Letters* **44**, 10 (2017).

28. G. A. Schmidt, *et al.*, *Geoscientific Model Development* **4**, 33 (2011).

29. A. P. Schurer, S. F. Tett, G. C. Hegerl, *Nature Geoscience* **7**, 104 (2014).

30. Core Writing Team, *Climate Change 2014: Synthesis Report* (Intergovernmental Panel on Climate Change, Geneva, Switzerland).

31. M. Katzfuss, D. Hammerling, R. L. Smith, *Geophysical Research Letters* **44**, 5720 (2017).

32. T. M. Lenton, V. Dakos, S. Bathiany, M. Scheffer, *Scientific reports* **7**, 5940 (2017).

33. J. Hansen, M. Sato, R. Ruedy, *Proceedings of the National Academy of Sciences* **109**, E2415 (2012).

34. L. Alexander, S. Perkins, *Environmental Research Letters* **8**, 041001 (2013).

35. C. Huntingford, P. D. Jones, V. N. Livina, T. M. Lenton, P. M. Cox, *Nature* **500**, 327 (2013).

36. S. Beguería, S. M. Vicente-Serrano, M. Tomás-Burguera, M. Maneta, *International Journal of Climatology* **36**, 3413 (2016).

37. P. Sherman, A. Archibald (2019).

38. B. Zhou, *et al.*, *Journal of Applied Meteorology and Climatology* **55**, 493 (2016).

Acknowledgments

This work has been supported by Studentships and Scholarships to A.K. (Natural Environmental Research Council, NE/L002485/1); M.I. (University of the Punjab Overseas Scholarship and UCL Overseas Research Scholarship). Guidance and encouragement from Serge Guillas, Kees Klein Goldewijk, Mark Maslin, Andrew Schurer and David Thornalley fostered and improved this research. We would also like to thank the Climate Monitoring and Attribution team at the Hadley Centre, the Climate Model Intercomparison Project members, those behind the History Database of the Global Environment collated by the Netherlands Environmental Assessment Agency, and the scientists at the Center for International Earth Science Information Network at Columbia University – without their generous efforts to create, curate and freely-release their databases, this research would not have been possible.

Supplementary materials

Materials and Methods

Figs. S1 to S6

Tables S1 and S2

References *(28-38)*

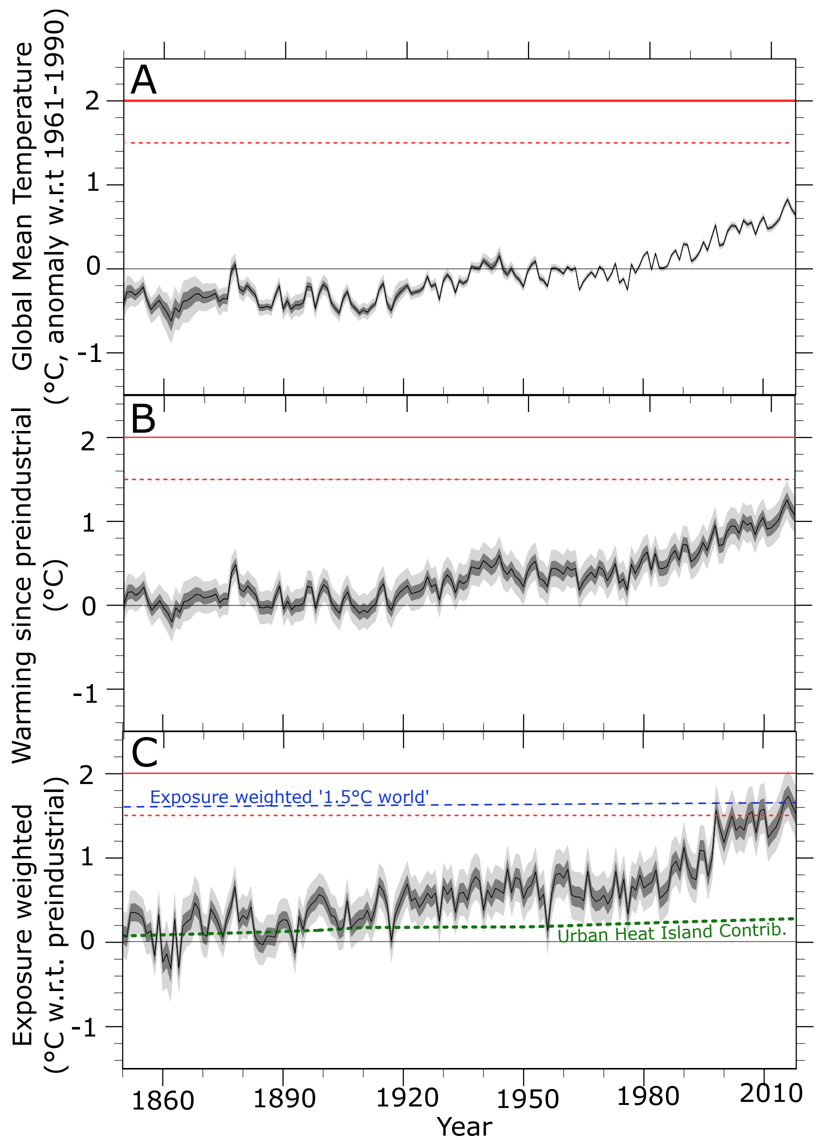

Figure 1: Global mean, annual average temperature change. The median, likely (33–66%) and 5–95% ranges (*7*) with respect to (A) the 1961–1990 CE climatological period and (B) the preindustrial. (C) The average global temperature weighted by exposure (*21*) (i.e. population, including an urban heat island adjustment). The dashed blue line shows the (median) equivalent of an exposure-wieghted 1.5 °C warmer world derived from pattern-scaling, and the dashed green line shows the (median) contribution from the urban heat island effect (Methods).

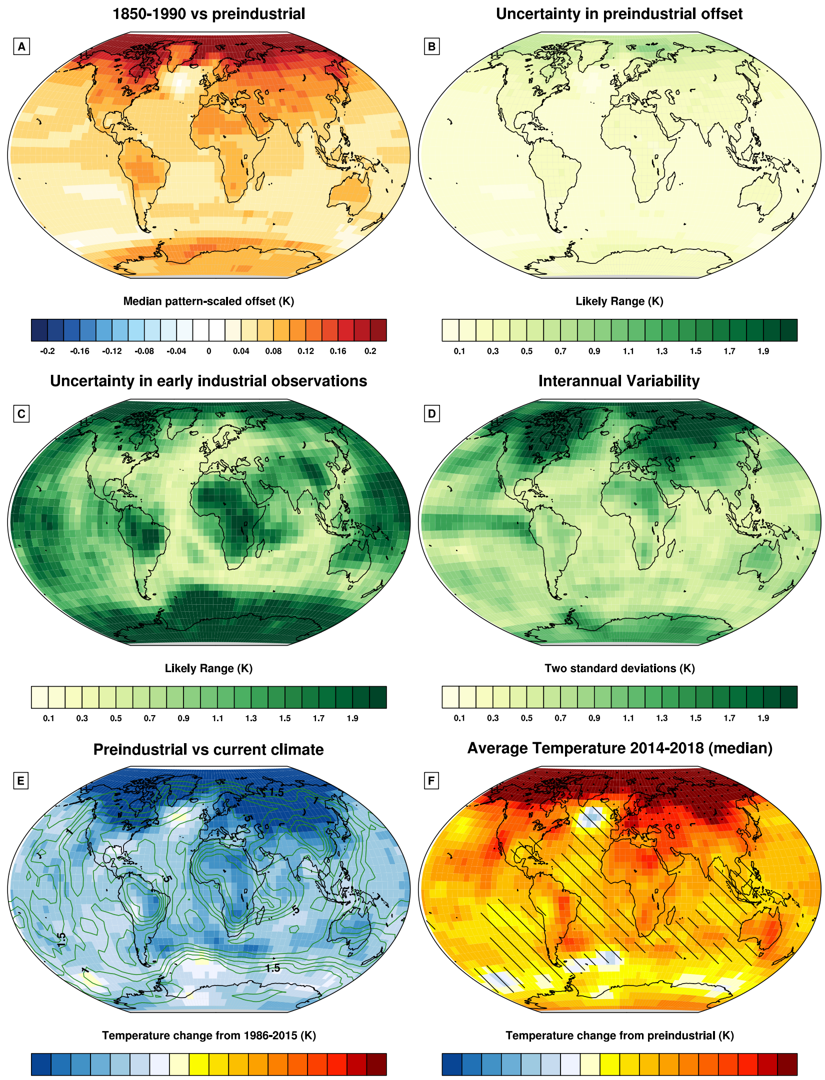

Figure 2: Spatial patterns of temperature change. (a) The median annual average offset of the preindustrial period from the 1961–1990 CE climatology, along with the interquartile range (green contours) in the offset. (b) The annual temperature of 2016 CE above preindustrial. Cross-hatching indicates regions that are not significantly different from the preindustrial at the 5% confidence level. Stippling shows regions that are at 1.5 °C or higher at the 5% confidence level.

MATERIALS AND METHODS

Observed Temperature Dataset

Teh initial temperature dataset used here is the Ilyas *et al.* (*7*) variant of HadCRUT4 (*10*). The HadCRUT4 data are a blend of surface air temperatures over land and sea surface temperature anomalies (*10*). It consists of an ensemble of 100 realisations that sample the observational uncertainties arising from the non-climatic signals. Unlike other prominent instrumental temperature records, these sparse spatial fields are not interpolated. Ilyas *et al.* (*7*) used a multi-resolution lattice kriging approach to quantify uncertainties arising from the lack of spatial coverage in HadCRUT4. The multi-resolution feature of the approach encapsulates variations from regional to global scale. As a result of this, the probabilistic local temperatures are expressed as a 10,000 member ensemble that samples both the observational and spatial uncertainties in the instrumental records. The uncertainty estimates in Fig. 1a are based on this spatially-complete dataset (*7*), and are slightly larger than previously estimated from the sparse coverage alone (*10*).

Preindustrial global mean offset

There is an established procedure to undertake a simulation covering the last millennium (*28*). This has enabled the creation of a multi-model ensemble, including some perturbed members designed to permit detection and attribution (*29*). Schurer *et al.* (*14*) use this 26-member ensemble to determine the additional forced component of warming that occurred between 1400–1800 CE and 1850–1900 CE. These 26 members are used to create a probability distribution function of the warming using kernel density estimation. This probability distribution function is then randomly sampled 10,000 times to determine the global mean offset for each member of the Ilyas *et al.* (*7*) observed temperature dataset. The mean difference between the preindustrial baseline (1400–1800 CE) and 1850–1900 CE is 0.076 °C with a 95% confidence interval of

-0.13 °C to 0.29 °C.

Pattern Scaling Method

Climate model runs of different scenarios and time horizons show consistent geographical patterns of projected warming (*30*). Pattern scaling methods can be used to infer projected changes to climate variables from existing model run results for alternative scenarios and time horizons. This is advantageous for ascertaining information of interest without requiring (impractical and often unfeasible) additional computationally-demanding climate model simulations (*18*). It is particularly suitable for approximation of large-scale regional average temperature changes due to the robustness of geographical temperature patterns and their modulation by corresponding global average temperatures changes (*30*). Pattern scaling applies only to climate variable patterns from external forcings while the real world response is a combination of natural variability and the external forcings. As the preindustrial global mean offsets (*14*) above represent a forced response over a multi-decadal period, this is not a problem in this situation. Here we describe a new pattern scaling approach that is grounded in a previous fingerprinting effort (*31*) used in detection and attribution of climate signals.

The input data used to create the scalable patterns in this work are a subset of the CMIP5 simulation output from the Earth System Grid Federation. They are a blend of annual surface air temperature over land and skin temperatures over the ocean from the RCP2.6 model runs (*14*). The blended temperatures have been regridded from their original resolution onto the 5° by 5° grid of the observations (*10*) through bilinear interpolation of the anomalies from 1961–1990 CE of their historical simulation. Only a single ensemble member is used for each climate model.

Pattern scaling relies on patterns emerging from external forcings rather than noise. Therefore, the blended annual surface temperature data was converted from annual data to 30-year climate means to eliminate some internal variability. Rather than each model being treated individually, the 30-year mean temperature anomalies from all runs were stitched together consecutively to form $\Delta T\left(c,\phi,\theta\right)$, where c is the 30-year climate instance, ϕ is the latitude and θ is the longitude. Principal component analysis was conducted on the stitched dataset to identify the principal component time series, w, of the empirical orthogonal function (EOF) regional surface temperature patterns, P (Fig. S1), as well as the variance explained by each EOF (Tab. S1). The simulated temperature anomalies can be reconstructed using only the first 10 principal components:

$$\Delta T\left(c,\phi,\theta\right)=P_{1\ldots10}\left(\phi,\theta\right)w_{1\ldots10}(c)+\varepsilon\left(c,\phi,\theta\right) \tag{1}$$

where $\varepsilon\left(c,\phi,\theta\right)$ represents the error in the reconstruction, which we subsequently treat as independent, gridpoint noise. The global mean temperature anomaly for each 30-year climate, $g(c)$, is calculated as the area-weighted average, $\langle\Delta T\left(\phi,\theta\right)\rangle$. Each principal component time series and the grid point noise are linearly regressed against the global mean temperature anomalies to extract the components relevant for pattern scaling:

$$\begin{gathered} w_i(c)\simeq\hat{r}_i.g(c) \\ \varepsilon\left(c,\phi,\theta\right)\simeq\hat{m}(\phi,\theta).g(c) \end{gathered} \tag{2}$$

where $\hat{x}$ represents an estimator with quantified uncertainties. The scaling factors for the leading 10 principal components are given in Tab. S1. The resultant scaled pattern for a forced, global mean temperature change of g is then:

$$\hat{O}_g=\left[\sum_{i=1\ldots10}\hat{r}_iP_i+\hat{m}\right].g \tag{3}$$

The benefit of this approach is that it generates scalable patterns which persist across different models. The first EOF, explaining around 85% of temperature variance (Fig. S1), is the

EOF	Variance explained (%)	Regression Coefficient (σ per °C)
1	85	2.158 (2.154 - 2.162)
2	3.1	0.0086 (-0.0038 - 0.021)
3	2.3	0.0138 (0.0002 - 0.0273)
4	1.5	0.0025 (-0.0094 - 0.0142)
5	0.66	-0.0004 (-0.0076 - 0.0065)
6	0.56	0.0002 (-0.0067 - 0.0072)
7	0.48	-0.0008 (-0.0073 - 0.0052)
8	0.46	-0.0001 (-0.0058 - 0.0058)
9	0.40	0.0002 (-0.0069 - 0.0072)
10	0.36	0.0004 (-0.0052 - 0.0062)

Table S1: Leading EOFs. The percentage variance explained by the 10 EOFs (Fig. S1), and the regression coefficients between their principal component time series and global mean temperature.

main regional temperature pattern from external forcings. Not all the EOFs describe the pattern from external forcings; some identify model differences, natural variability, or noise. The uncertainties in the regression slopes are randomly sampled 10,000 times to create a scalable pattern for each of the ensemble members of the rebased Ilyas *et al.* dataset (*7*). This procedure creates and samples the local/global ratio of temperature increases, whilst maintaining the spatial covariance structure. After multiplying each scalable pattern by the sampled preindustrial global mean offset (originally from Schurer *et al.* (*14*)), it is possible to calculate the additional warming that had occurred in the early instrumental period (1850–1900 CE) since the preindustrial (1400–1800 CE). The median estimate of the forced temperature changes that occurred between the preindustrial and the early industrial is a slight warming everywhere (Fig. 2A), with a likely range that often encompasses both positive and negative temperature changes (Fig. 2B).

Each ensemble member of the Ilyas et al. dataset (*7*) is converted from its original 1961-1990 reference period to a preindustrial one by first removing the average value of 1850-1900 and then removed realisation of the pattern-scaling response prior to instrumental observations.

Alternate versions to Fig. 3 and Fig. 4 that use the early industrial reference period are provided as Fig. S5 and Fig. S6 respectively.

Interannual Variability and Signal Emergence

The impacts and perceptions of climate change are not only determined by changes in the long-term mean (*24*). It is necessary to also recognise the sensitivity of society and ecosystems to climate variations and extremes (*32*). One such form of climate variation is the variability of annual mean temperatures. The perception of persistently high climate variability is perhaps one of the biggest barriers to recognise and understand long-term climate change trends (*33*). The current body of literature fails to conclusively answer whether interannual variability is increasing globally, but observation-based studies appear to indicate little change in global annual mean temperature variability (*34, 35*). After Huntingford *et al.* (*35*), we compute interannual temperature variability as the long-term average of the 11-yr standard deviations after detrending the annual temperature anomaly data using a local 11-yr running mean. Fig. 2D shows the interannual variability for 1986-2015. S3, mean levels of variability before and after 1986 are shown. We identify no clear overall positive or negative trend in interannual variabiility from the Ilyas *et al.* dataset (Fig. S3. Contrary to Huntingford *et al.* (*35*), we find strongly positive changes over the tropics, especially over Amazonia, whilst we see little increases in variability over Europe. Whilst some of this difference probably arises from the longer records in our analysis, the more rigorous treatment of uncertainties during interpolation used in this study may be the underlying cause (*36*). Nonetheless, for the purposes of population exposures in Fig. S4, the interannual variability taken from Fig. 2D and kept constant with time.

Demography, Urbanisation and the Urban Heat Island

The primary database (*19*) used for population information is HYDE 3.2. This database provides estimates of total population, rural population and urban population at 5' resolution across the globe since before 1850 CE. The temporal resolution is only annual in the most modern portion, so linear interpolation is used over the decadally-resolved portions. This database has been derived from a combination of census information at national scales and sub-national scales, combined with some distributional modelling (*19*).

The temperature consequences of urbanisation is estimated using the Global Urban Heat Island Dataset (*23*). This consists of two pairs of satellite-based temperature observations from within and outside urban centres averaged over the summer of 2013 CE. The daytime and nighttime differences are averaged and presumed to provide an annual mean offset. This dataset has been similarly used to look at population exposure under future projections (*37*). Variations of the urban heat island effect (UHIE) over the course of the year do not demonstrate a consistent seasonal cycle across the globe (*38*). Therefore, we consider this to be a smaller source of error than the assumption that 2013 CE is representative of every year since 1850 CE. This latter assumption is unavoidable as no global dataset yet exists to provide such information. In theory, it may be possible to create such a dataset from the adjustments made during the creation of HadCRUT4 (*10*). However in practice the homogenisation algorithm has not been designed in a way that allows even the feasibility of such an approach to be tested. The UHIE in this work therefore ends up being a spatially-varying, but temporally constant, adjustment applied only to the urban population in each gridcell.

Quantified errors are not available for either the urban heat island effect (*23*) or demographic trends (*19*), so the uncertainty presented in the figures relates solely to the temperature estimate. It is unclear how the urban heat island effect should be accounted for when converting from local temperatures to their global-mean equivalents. We use slightly different approaches for

Fig. 1 and Fig. S4 given their different meaning. In Fig. 1c, the exposure-weighted '1.5 °C world' (blue reference line) is computed without the urban heat island effect, because it is solely intended to provide the reader an indication of the consequences of the population not being spread uniformly across the globe. However in Fig. S4 the UHIE is included in the calculation of global-mean equivalent, as it is rather a measure of peoples exposure to warmer temperatures.

Data and Code Availability

The original Ilyas et al (*7*) dataset is available at `https://oasishub.co/dataset/global-monthly-temperature-ensemble-1850-to-2016`. The code repository used to create all the results and figures shown in the manuscript is `https://bitbucket.org/cbrierley/experience_1pt5/src/master/`.

Author contributions statement

CB conceived the project, performed the analysis, and wrote the manuscript with AK. AK processed the HYDE population dataset, created the cartograms and devised the urban heat island adjustment with CB. MI developed the various sampling techniques used. NW devised the pattern-scaling approach. JK undertook the comparison with interannual variability.

Additional information

The authors declare no competing interests.

a). 2015	$\leq 0°C$	$\geq 1°C$	$\geq 1.5°C$	$\geq 1.5°C$*	$\geq 2°C$
Local warming (1400-1800)	0.5 (0.1- 2.1)	79.1 (69.8-87.7)	54.8 (45.7-65.2)	40.1 (29.7-51.8)	31.9 (24.9-40.0)
Global warming (1400-1800)	0.5 (0.1- 2.1)	77.4 (68.3-87.3)	50.0 (40.6-60.3)	34.6 (24.3-45.8)	24.5 (18.4-32.1)
Local warming (1850-1900)	0.7 (0.3- 2.5)	75.5 (67.5-83.9)	50.4 (43.7-59.1)	34.8 (27.3-44.1)	28.2 (23.3-34.7)
Global warming (1850-1990)	0.7 (0.3- 2.5)	73.4 (66.1-82.8)	45.3 (38.3-53.4)	29.3 (21.8-38.2)	21.1 (17.0-26.7)
Area of globe (1400-1800)	*10.2 (7.9-12.7)*	*54.6 (48.4-60.5)*	*31.0 (26.2-36.1)*	*N/A*	*17.2 (14.0-20.7)*
b). 2014-2018	$\leq 0°C$	$\geq 1°C$	$\geq 1.5°C$	$\geq 1.5°C$*	$\geq 2°C$
Local warming (1400-1800)	0.8 (0.2- 2.3)	77.9 (68.1-86.3)	52.8 (43.3-63.7)	38.6 (28.4-50.6)	29.5 (22.4-38.0)
Global warming (1400-1800)	0.8 (0.2- 2.3)	76.8 (66.2-86.2)	46.3 (36.4-58.0)	29.5 (19.1-42.2)	20.5 (15.1-27.6)
Local warming (1850-1900)	1.1 (0.3- 2.7)	74.2 (65.4-82.1)	48.5 (41.0-57.6)	33.7 (25.8-42.8)	25.7 (21.0-32.3)
Global warming (1850-1990)	0.8 (0.2- 2.3)	76.8 (66.2-86.2)	46.3 (36.4-58.0)	29.5 (19.1-42.2)	20.5 (15.1-27.6)
Area of globe (1400-1800)	*7.4 (5.3- 9.8)*	*51.3 (44.8-57.9)*	*27.3 (22.5-32.4)*	*N/A*	*14.1 (10.9-17.4)*

Table S2: The percentage of the global population exposed to various temperature classes in (a) 2015 and (b) 2014-2018. Values are given for both the local and global-mean equivalent temperatures, with respect to both the preindustrial (1400-1800 CE) and early industrial (1850-1900 CE). In brackets is the likely range of each value (i.e. containing two-thirds of the ensemble members). The percentage of the global area (rather than the population) are shown italics. *This column shows the results of performing the calculation without inclusion of the urban heat island effect.

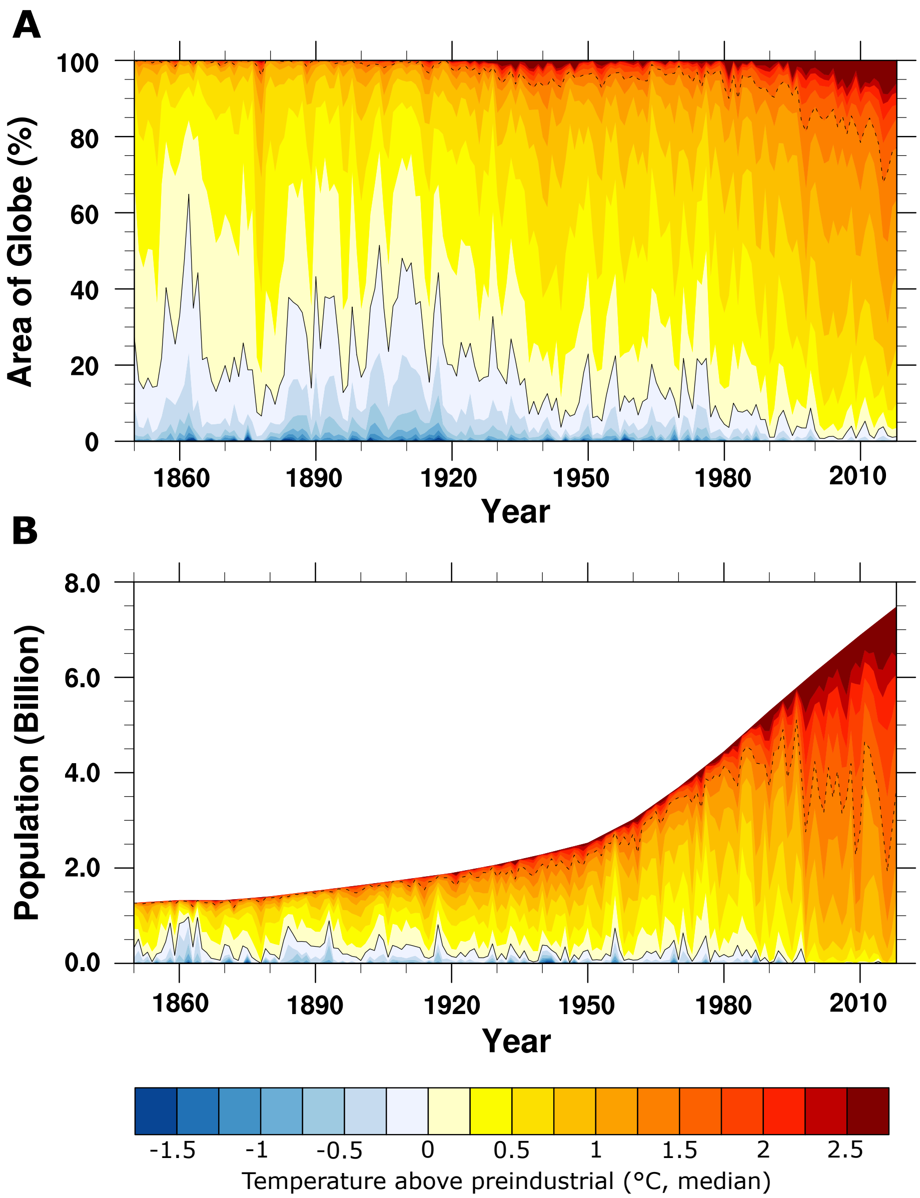

Figure 3: Subdividing global area and population by warming. (a) The proportion of the global area at particular (median) annual temperatures in each year. (b) The population (*19*) exposed to particular (median) annual temperatures in each year since 1850 CE. The preindustrial and +1.5 °C are indicated by black solid and dashed lines respectively.

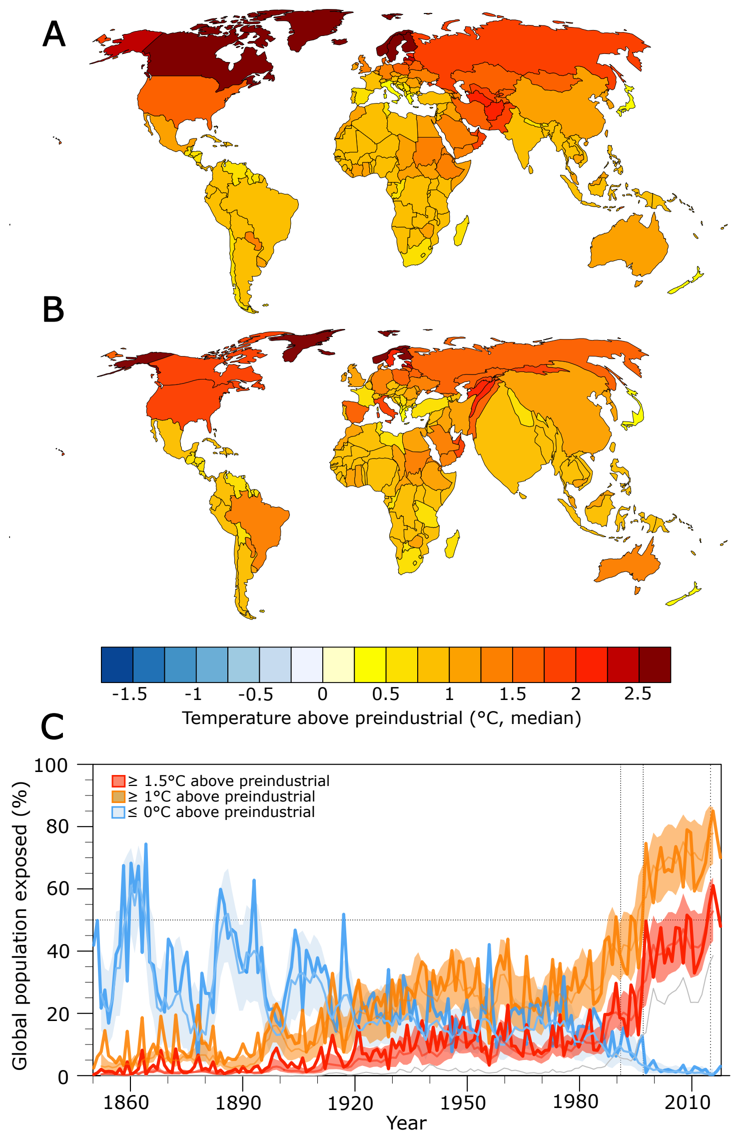

Figure 4: Exposure to annual mean temperatures. (A) Conventional cartogram, where a nation is coloured according to its 2014-2018, median, area-averaged temperature anomalies. (B) An exposure-weighted cartogram, where a country's size is determined by its population (*26*), and the colour is the exposure-weighted temperature anomaly incorporating the urban heat island (median, 2014-2018). (C) The proportion of the global population exposed to various temperature levels with respect to the preindustrial. The thick line shows the annual median value, whilst the thin lines show the 5-year running median temperature estimates along with its likely range. The grey line shows the +1.5 °C exposure without considering the urban heat island. Dotted vertical lines indicate major international commitments to tackle climate change in 1992 CE (Rio), 1997 CE (Kyoto) and 2015 CE (Paris).

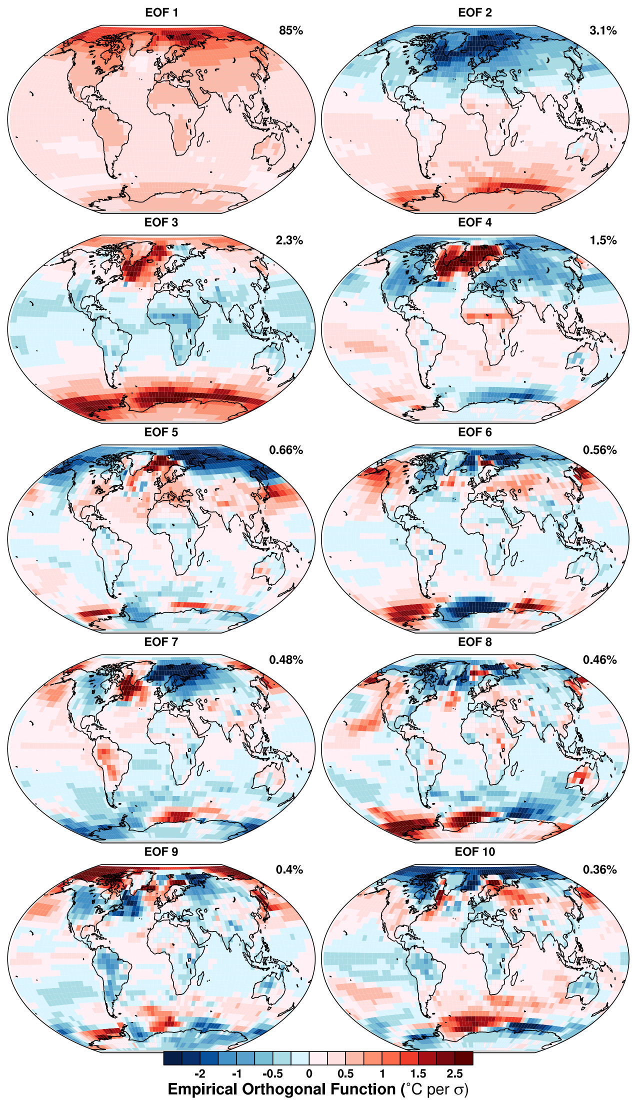

Figure S1: The leading EOFs of changes in 30-year averaged temperature change simulated by models participating in CMIP5 under the historical and RCP2.6 scenarios. The percentage of variance explained by each pattern is also shown.

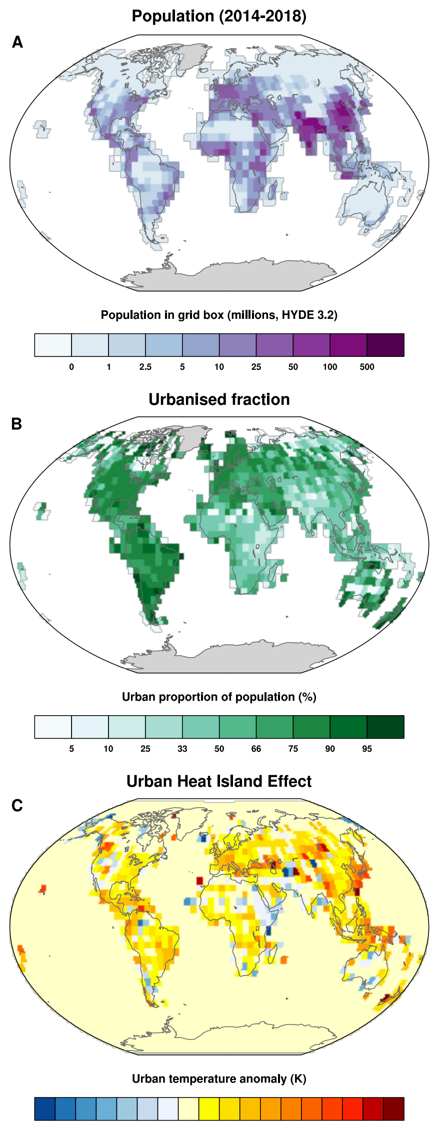

Figure S2: Population and urbanisation. (A) The total population of contained within a grid box (*19*) averaged between 2014-2018 CE. (B) The percentage of that population that is urban. (C) The difference in temperature between urban and rural locations averaged over each grid box during summer 2013 (*23*).

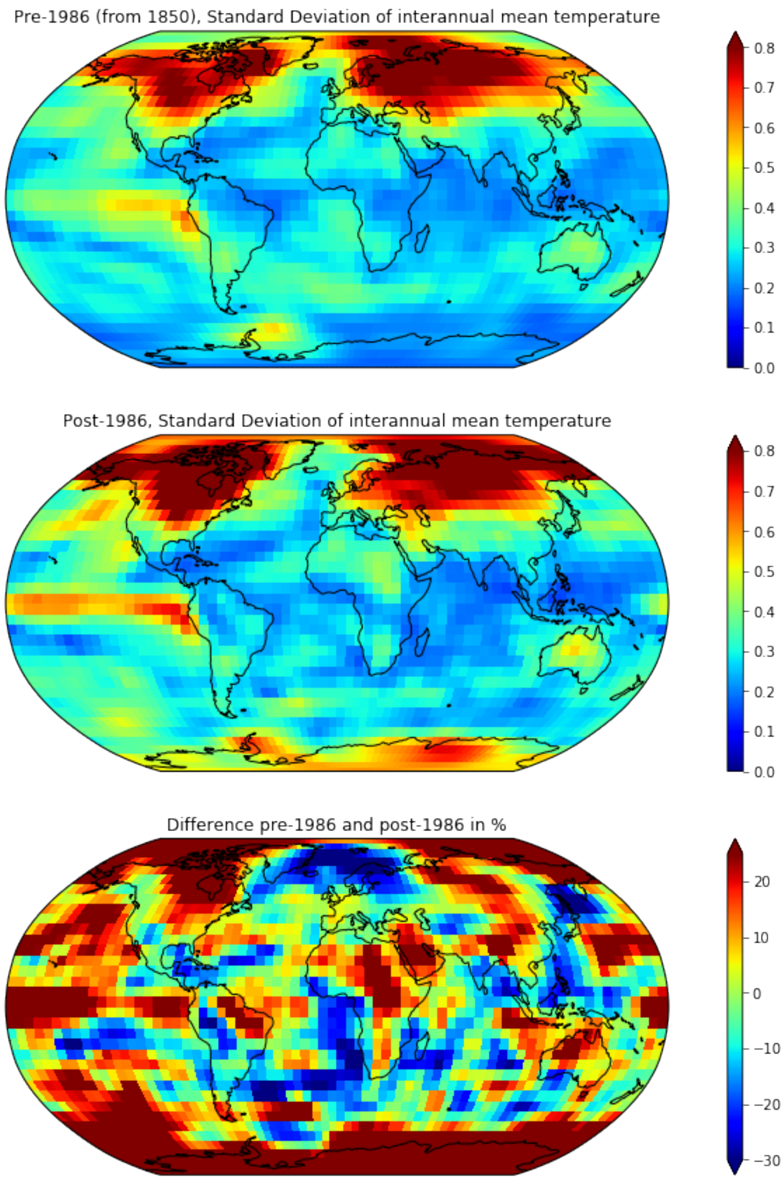

Figure S3: Local interannual mean temperature variability. Annual standard deviations are calculate over 11-yr detrended periods. Local means of this standard deviation are plotted for the period on the record before 1986 and after 1986. The local change between the two time periods is shown in percentages.

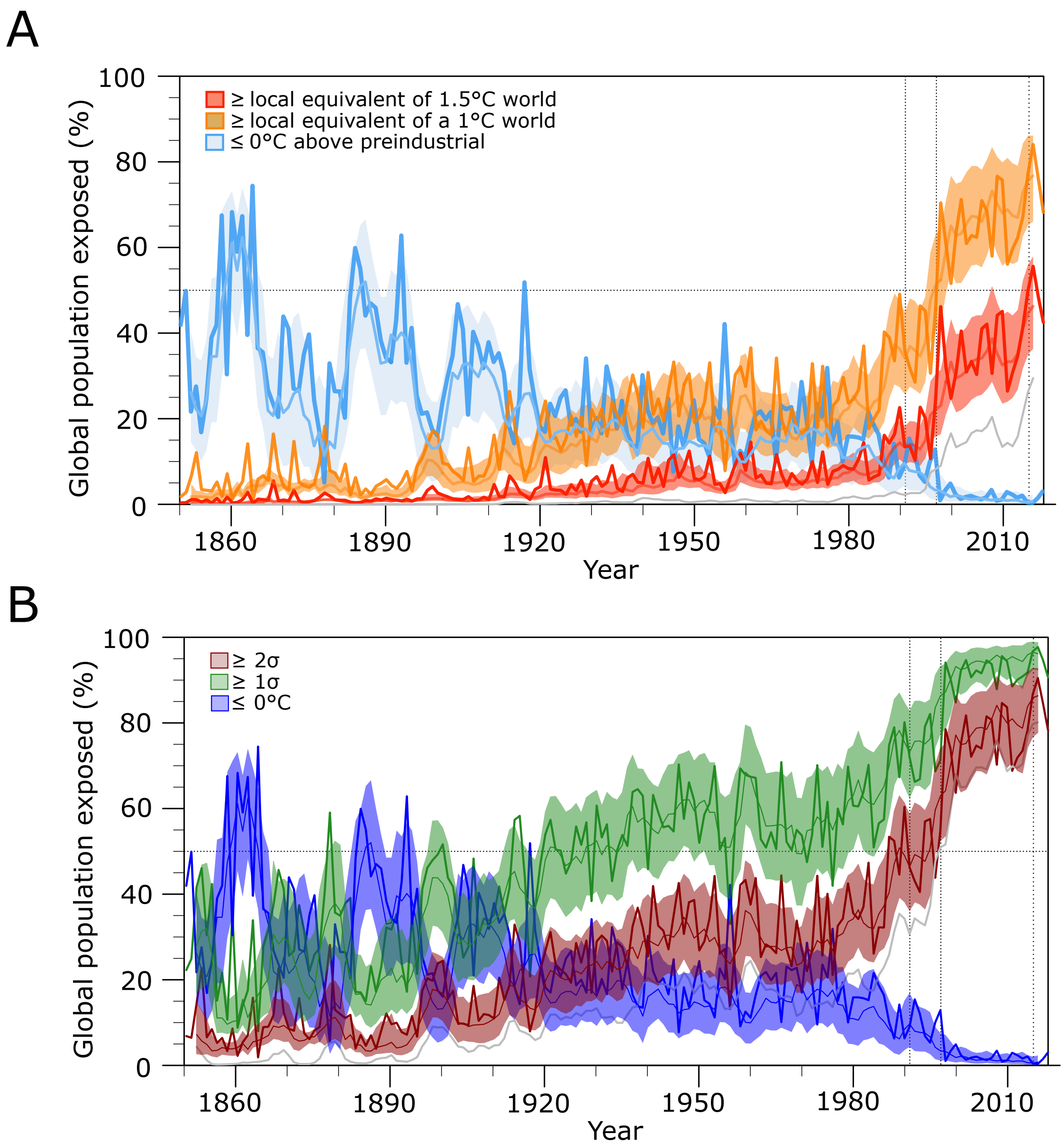

Figure S4: Alternative exposure time series. (A) The proportion of the global population exposed to local equivalents of *global mean* temperatures above preindustrial. (B) Given that interannual variability differs across the globe (Fig. 2D), local exposure may be better measured in units of standard deviations rather than warming directly. The thick line shows the annual median value, whilst the thin lines show the 5-year average median temperature estimates along with its likely range. The grey line shows the +1.5 °C (or 2σ) exposure, without considering the urban heat island. Dotted vertical lines indicate major international commitments to tackle climate change in 1992 CE (Rio), 1997 CE (Kyoto) and 2015 CE (Paris).

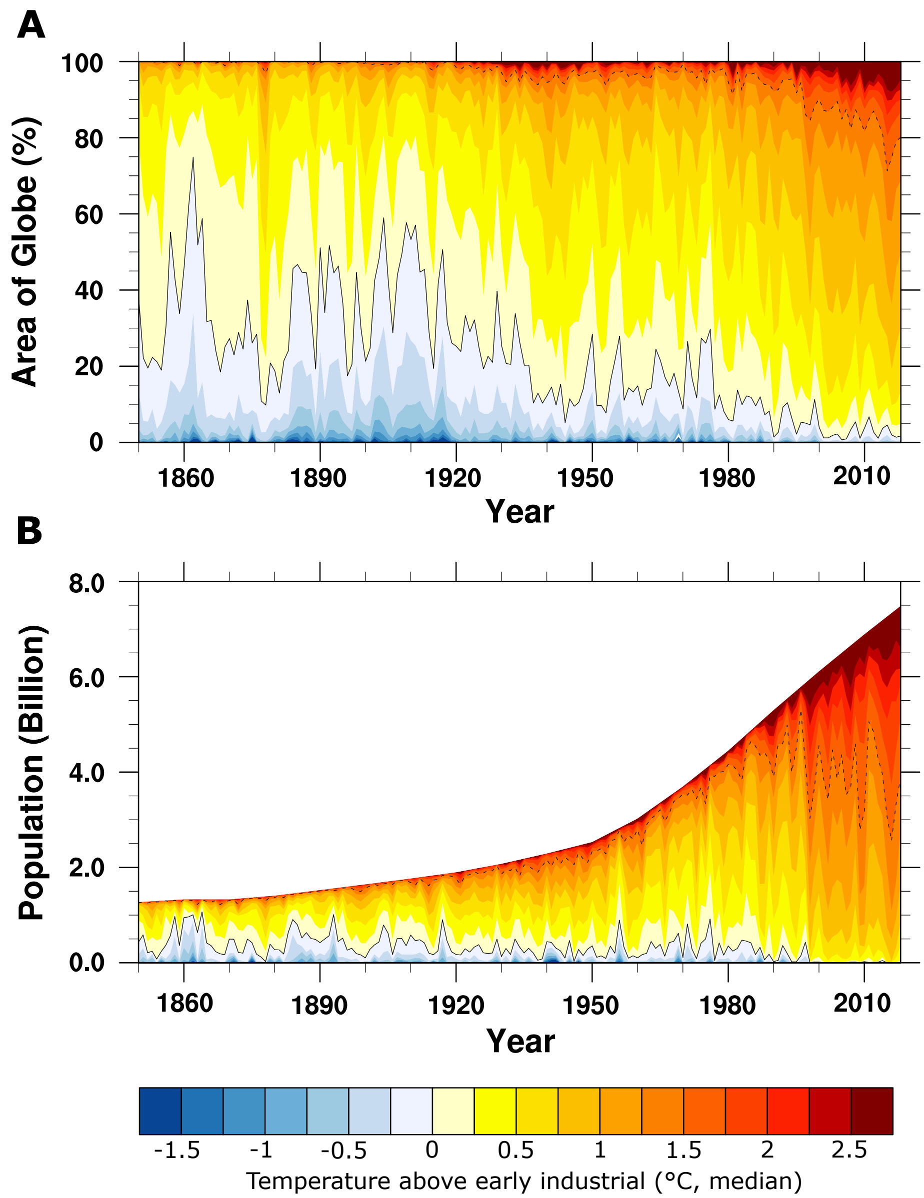

Figure S5: Subdividing global area and population by warming since the early industrial. (a) The proportion of the global area at particular (median) annual temperatures in each year. (b) The population (*19*) exposed to particular (median) annual temperatures in each year since 1850 CE. The preindustrial and +1.5 °C are indicated by black solid and dashed lines respectively.

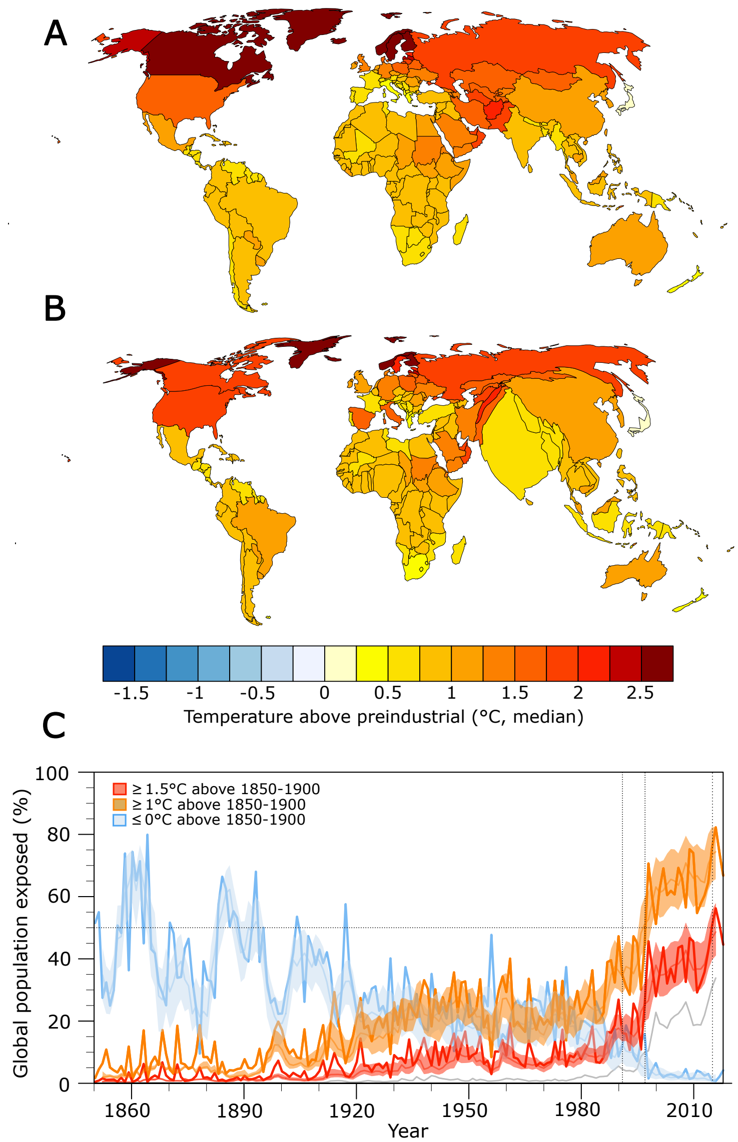

Figure S6: Exposure since the early industrial. This is an alternate version of Fig. 4 using a baseline of 1850-1900, rather than preindustrial. (A) Area-averaged cartogram. (B) Exposure-weighted cartogram. (C) The proportion of the global population exposed to various temperature levels. The grey line shows the +1.5 °C exposure without considering the urban heat island.